Tracking the Cracking: a Holistic Analysis of Rapid Ice Shelf Fracture Using Seismology, Geodesy, and Satellite Imagery on the Pine Island Glacier Ice Shelf, West Antarctica

S. D. Olinger[1,2], B. P. Lipovsky[2], M. A. Denolle[2], B. W. Crowell[2]

[1]Department of Earth and Planetary Sciences, Harvard University, Cambridge, Massachusetts, USA
[2]Department of Earth and Space Sciences, University of Washington, Seattle, Washington, USA

Key Points:

- Fracture at PIG generate flexural gravity waves, a wave type related to interaction between a floating plate and supporting fluid.
- Rift-tip seismicity rate increases with ice speed, either due to changes in the underlying ice shelf stress state or localized thinning.
- Recorded flexural gravity waves are consistent with a point load of ∼10 kPa applied over ∼30 s, corresponding to ∼10 m of vertical cracking.

Corresponding author: Stephanie D. Olinger, `stepholinger@fas.harvard.edu`

Abstract

Ice shelves regulate the stability of marine ice sheets. We track fractures on Pine Island Glacier, a quickly-accelerating glacier in West Antarctica that contributes more to sea level rise than any other glacier. Using an on-ice seismic network deployed from 2012 to 2014, we catalog icequakes that dominantly consist of flexural gravity waves. Icequakes occur near the rift tip and in two distinct areas of the shear margin, and TerraSAR-X imagery shows significant fracture in each source region. Rift-tip icequakes increase with ice speed, linking rift fracture to glaciological stresses and/or localized thinning. Using a simple flexural gravity wave model, we deconvolve wave propagation effects to estimate icequake source durations of 19.5 to 50.0 s, and transient loads of 3.8 to 14.0 kPa corresponding to 4.3 to 15.9 m of crevasse growth per icequake. These long source durations suggest that water flow may limit the rate of crevasse opening.

1 Plain Language Summary

Large shelves of floating ice strengthen glaciers in Antarctica, helping to protect against rapid sea level rise that can occur when glaciers flow into the ocean. Ice shelves can collapse through rapid cracking (synonym of fracturing), but it is difficult to directly observe cracking on ice shelves. In this paper, we track cracks on Pine Island Glacier, an ice shelf in Antarctica that is particularly vulnerable to collapse. We see cracks in pictures taken by satellites. Cracking causes the ice shelf to shake up and down, which we record using the same equipment that records earthquakes. We record shaking located at a set of cracks at the side of the ice shelf and at the tip of a single massive crack called a rift. Rift cracking seems related to the speed that the ice shelf is flowing. We also use a computer simulation of shaking to learn about the details of the crack process. Our simulation suggests that the crack process might be more complicated than a single crack opening evenly at a constant rate.

2 Introduction

Ice shelf fracture exerts a fundamental control on the stability of marine ice sheets and associated sea level fluctuations (Seroussi et al., 2020). In particular, understanding the past, present, and future stability of the West Antarctic Ice Sheet (WAIS) remains one of the great challenges of modern glaciological research and is itself closely related to ice shelf fracturing processes (Scambos et al., 2017). Fractures on ice shelves take on many forms including through-cutting rifts (Larour et al., 2004; Hulbe et al., 2010; Lipovsky, 2020), smaller-scale basal and surface crevasses (Rist et al., 2002; McGrath et al., 2012), hydraulic fracturing (Weertman, 1973; Banwell et al., 2013), and cliff failure (Clerc et al., 2019). Despite decades of progress, understanding of ice shelf fracture remains significantly hindered by a lack of direct observation (Benn et al., 2007). A number of basic questions remain or have only partially been addressed: What forces are involved in ice shelf fracture? Is ice shelf fracture a fast and brittle or slow and ductile process? To what degree is water involved in fracture propagation? Does ice shelf fracture growth happen at a constant rate or in bursts, and what controls its timing?

All of these questions can be addressed using seismology. Because seismic waves carry information about the dynamics of fracture, numerous previous studies have leveraged such signals, referred to as icequakes, for this purpose (Von der Osten-Woldenburg, 1990; Hammer et al., 2015; Chen et al., 2019; Winberry et al., 2020). Seismic studies on ice shelves have shown that crevasse propagation is intermittent (Bassis et al., 2007; Heeszel et al., 2014) and have highlighted environmental forcings that would be difficult to ascertain using only remotely sensed observations (Bassis et al., 2008; Olinger et al., 2019; Aster et al., 2021).

Here, we use seismic recordings to quantify fracturing of Pine Island Glacier (PIG) Ice Shelf. PIG, part of the larger WAIS, contributes more to present day global sea level rise than any other glacier (Shepherd et al., 2018). Current ice mass loss at PIG is thought to be due to the retreat of the floating ice shelf (Joughin, Shapero, Smith, et al., 2021) being caused by interactions between ocean forcing (Christianson et al., 2016; Joughin, Shapero, Dutrieux, & Smith, 2021) and fracturing processes (MacGregor et al., 2012).

We focus on icequakes that travel as flexural gravity waves to quantify fracturing of PIG Ice Shelf. Flexural gravity waves are a type of hybrid seismic-water wave (Ewing & Crary, 1934) unique to floating structures such as ice shelves since both elasticity and buoyancy act as their restoring force (Ewing & Crary, 1934). Flexural gravity waves are strongly dispersive (Ewing & Crary, 1934), which can make waveform analysis difficult and necessitates careful modelling (Sergienko, 2017; Mattsson et al., 2018; Lipovsky, 2018). Despite this challenge, flexural gravity waves are useful tools to study ice shelf processes because, while direct body waves in ice shelves are often not observed at distances greater than a few ice thickness (Zhan et al., 2014), flexural gravity waves are often observed to travel long distances from their exciting source (Williams & Robinson, 1981).

Many sources generate flexural gravity waves on ice shelves including ocean swell (Williams & Robinson, 1981), tsunamis (Bromirski et al., 2017), and airplane landings (MacAyeal et al., 2009). MacAyeal et al. (2009) appears to have been the first to propose that fracturing processes in ice shelves may act as seismic sources that generate flexural gravity waves. MacAyeal et al. (2009) considered water motion in a deforming rift and motion of detaching blocks from the ice front as two such sources. Here, we hypothesize that crevasse growth generates flexural gravity waves.

We begin our fracture analysis by describing a timeline of events with the use of satellite imagery. Next, we catalog flexural gravity waves on PIG to examine the relationship between crack growth, large-scale rift propagation, shear margin processes, and ice shelf acceleration. We then interrogate icequake source physics by modeling the ice shelf as a buoyantly supported beam, the simplest model that captures flexural gravity wave propagation (Sergienko, 2017; Mattsson et al., 2018). In our analysis, we model flexural gravity wave generation by a point load or bending moment applied during ice shelf crevasse growth to infer key source parameters of the recorded icequakes.

3 Analysis of Satellite Imagery and Positioning

We track visible fracturing on PIG using images collected by the TerraSAR-X satellite (Pitz & Miller, 2010) from 2012 to 2014. At the start of our study period in January 2012, the primary visible fractures are the rift, ~20 large cracks extending into the ice shelf from northern shear margin, and ~10 cracks extending into the ice shelf at the southern edge of the nascent iceberg (Figure 1a, left). By January 2013, the rift had propagated a few kilometers without significant widening, and two wing cracks (Renshaw & Schulson, 2001) opened at the rift tip (Figure 1a, right). One of the cracks at the northern shear margin extended 7 km and connected to the rift between May 8 and May 11, 2012. The other northern shear margin cracks extended and widened, at least two new cracks initiated near Evans Knoll, and one of cracks at the southern edge of the nascent iceberg extended to within a kilometer of the rift tip.

During the first four months of 2013, the wing cracks near the rift tip extended and widened. In early July 2013, a block of ice calved along a wing crack at the southern edge of the nascent iceberg near the rift tip (Figure 1b). After this preliminary calving event, the only connection between the nascent iceberg and the ice shelf was a 2 km wide strip of ice between the ocean and a wing crack. Over the next few months, we observe significant widening of the rift, likely due to the iceberg beginning to drift away from the ice shelf. Iceberg B-31 calved in November 2013 (Figure 1c) when left lateral motion of

the iceberg pried open a large wing crack near the rift tip until a strip of ice stabilizing
the iceberg broke off, allowing Iceberg B-31 to drift into the sea. By the end of 2013, many
fractures in the northern shear margin had extended and calved smaller icebergs, and
several new fractures had initiated near Evans Knoll.

We examine Global Positioning System (GPS) speed timeseries derived from five
continuous GPS stations. The GPS stations were co-located with seismometers (loca-
tions shown in Figure 2). Our GPS processing is described in Supporting Text S1. Fig-
ure 3a plots the GPS-derived ice shelf speed. We find that ice speed at PIG decreases
from 11.1 m/day in January 2012 to 10.8 m/day in April 2013. Then, ice speed drops
to below 10.6 m/day for eight days in early May 2013. Following this rapid slowdown,
ice speed begins to increase, reaching 10.9 m/day by the end of 2013. The GPS ice speed
we compute here is consistent with a previous study utilizing the same dataset (Christianson
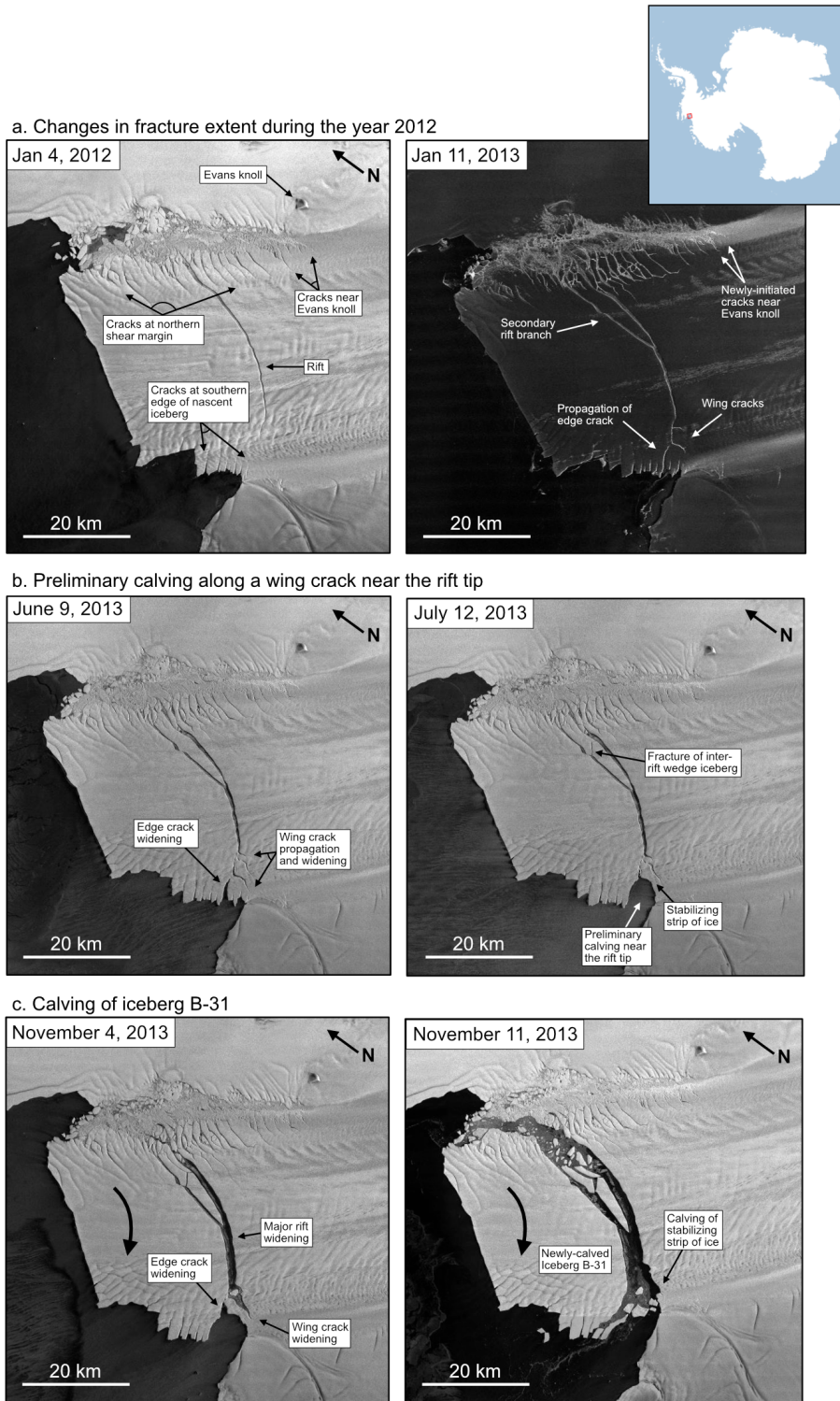et al., 2016).

4 Analysis of Seismograms

We examine seismic data from five sites on PIG (Stanton et al., 2013). The instru-
ments were deployed in January 2012 and retrieved in December 2013, providing two years
of continuous data. The seismic stations were deployed in a cross shape with 5 km aper-
ture at the center of the ice shelf (Figure 2). Each site consisted of a three component
Nanometrics Trillium 120 Broadband seismometer and a Quanterra Q330 digitizer (David
Holland & Robert Bindschadler, 2012). Seismic data was sampled at 100 Hz, and we re-
moved the instrumental response on the frequency band 0.001 Hz to 45 Hz.

In the seismic dataset, we observe events with an abrupt onset and with high fre-
quencies that arrive before low frequencies. This type of dispersion is characteristic of
flexural gravity waves. The observed dispersion (high frequency waves travel faster) is
the opposite of typical surface waves in the solid Earth. In the latter case, low frequency
waves travel faster because seismic wave speeds generally increase with depth.

To detect flexural gravity waves in the dataset, we design a two-stage detection scheme
that identifies broadband, dispersive seismic events. Our detection approach, detailed
in Text S2, uses a dual-band short term average/long term average (STA/LTA) detec-
tor in combination with template matching (Allen, 1978; Gibbons & Ringdal, 2006) to
detect a preliminary catalog of 22,119 events. Inspection of the preliminary catalog re-
veals two main families of events: one with clear high-frequency-first dispersion and one
which is dominantly monochomatic. To isolate flexural gravity waves, we undertake wave-
form clustering using a K-Shape algorithm (Paparrizos & Gravano, 2016) modified to
operate on multi-component seismic data. Visual analysis of the clustered catalog demon-
strates the efficacy of our approach in isolating flexural gravity waves (Figure 3). Our
final catalog contains 8,184 likely flexural gravity wave events, which we refer to as ice-
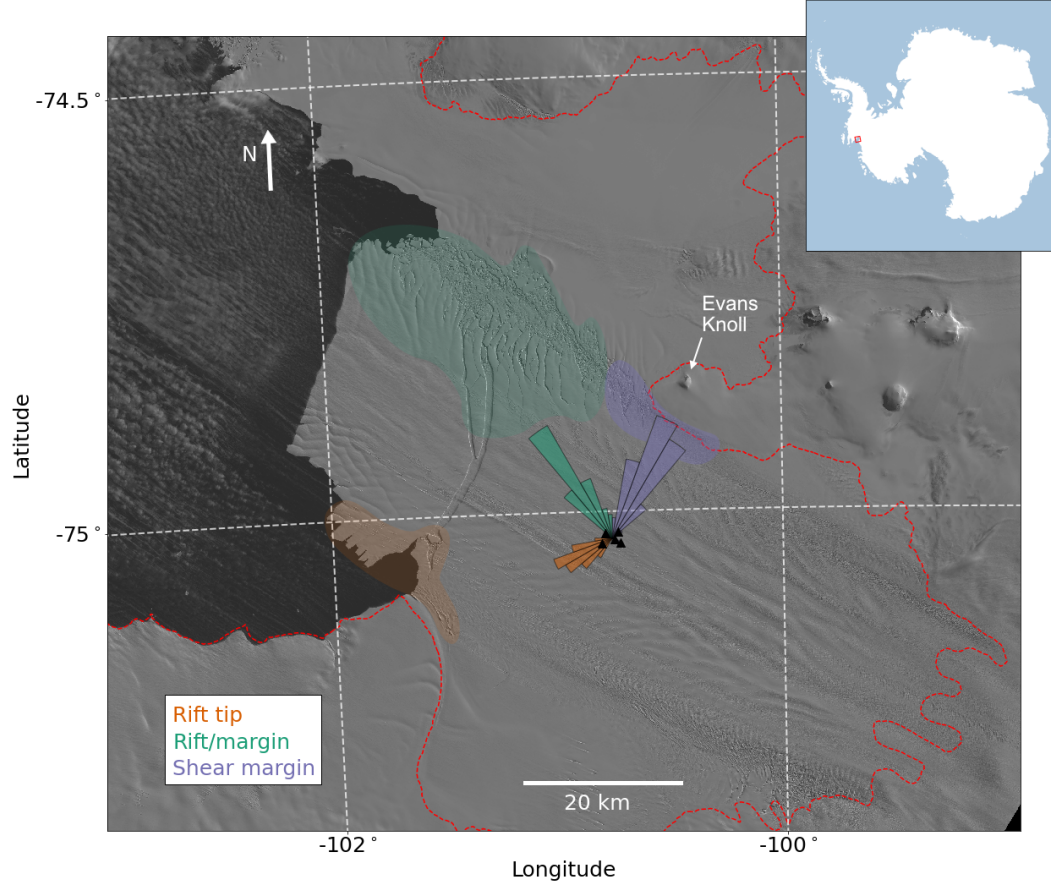quakes in the rest of the text.

We next determine locations for all icequakes in our final catalog. Given the poor
distribution of the stations with respect to fracture locations, we employ single-station
approaches to locating icequakes. We compute epicentral back-azimuths by analyzing
the polarization direction of recorded horizontal waves (Aster et al., 2021). We apply prin-
ciple component analysis (PCA) to the horizontal component seismograms to retrieve
polarization directions. The polarization provides a 180 degree ambiguity, so we find the
direction of propagation based on which station recorded the first arrival (see Text S3).

We locate all of the 8,184 icequakes to one of three distinct source regions: the rift
tip, the body of the rift and nearby shear margin ("rift/margin"), and the northeast shear
margin near Evan's knoll ("shear margin"), which are depicted in Figure 2. These spa-
tial groups correspond to 22%, 29%, and 40% of the catalog, respectively, with 9% of events

Figure 1. TerraSAR-X images showing an overview of fracture development at PIG from 2012 to 2014. Large arrow in panels c. and d. show sense of motion of the iceberg. See text for full discussion. Inset shows the location of PIG in Antarctica.
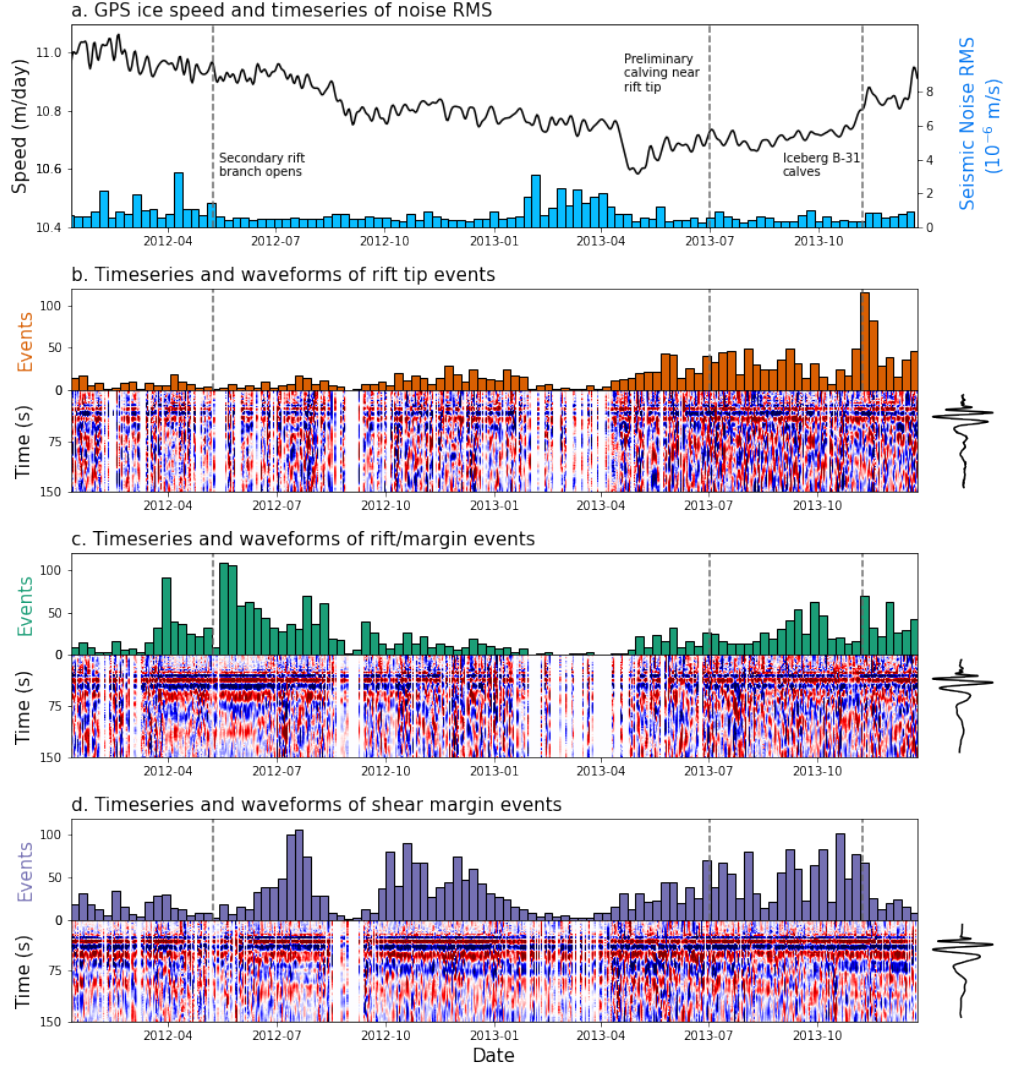
Figure 2. Back-azimuthal histogram showing locations of cataloged icequake. Rift-tip event back-azimuths are plotted as orange rays. Rift/margin event back-azimuths are plotted as green rays. Shear-margin event back-azimuths are plotted as purple rays. Likely source regions are shown by colored polygons. PIG array seismic and GPS stations are plotted as black triangles. Approximate grounding line position is shown by the red dashed line (Bindschadler et al., 2011). Background LANDSAT imagery is from October 2013 (courtesy of the United States Geological Survey).

having indeterminate locations. Figure 2 shows the back-azimuthal histograms of the three groups.

5 Relationships Between Icequakes and Ice Shelf Behavior

5.1 Rift tip

The rift-tip icequakes are coincident in space and time with several fracturing processes including rift propagation, wing cracking, small scale calving within the rift, and calving along the southern edge of the nascent iceberg. Rift tip events occurred more frequently in 2013 than in 2012 (Figure 3b). The mean seismicity rate was 9.4 icequakes/week in 2012 and 25.6 icequakes/week in 2013. 19 weeks of 2013 equaled or exceeded the maximum 2012 seismicity rate of 29 icequakes/week. Weekly icequake counts increased past the peak level seen in 2012 on May 21, 2013 and remain elevated until the end of the de-

Figure 3. Timing and waveforms of cataloged icequake. (a) GPS-derived ice velocity is shown by the black line, and average seismic noise is shown by blue bars. Noise is highest in the Antarctic summer, when minimal sea ice is present to attenuate ocean-generated noise, reducing detectability in January, February, and March. (b) Rift-tip events. Weekly timeseries of rift tip event times is shown by orange bars. Daily vertical (HHZ) waveform stacks of detected rift tip events are plotted beneath. Overall rift-tip event stack is shown to the right. (c) Same as (b) for rift/margin events, color-coded in green. (d) Same as (b) for shear-margin events, color-coded in purple.

ployment. This period of elevated rift tip seismicity corresponds to the phase of significant wing crack growth and rift widening observed in imagery. Rift tip icequakes appear located ~15 degrees south of the rift tip's position in LANDSAT imagery from October 12, 2013 (Figure 2). However, when Iceberg B-31 calved in November 2013, the wing crack extending south of the rift had propagated to a location consistent with the peak in the back-azimuthal distribution of rift tip icequakes (Figure 1c, left).

Peak levels of rift-tip seismicity were observed during the calving of Iceberg B-31 in the week of November 5, 2013. That week had 115 rift-tip events, the highest event count of any week across all three source regions. Furthermore, elevated rift-tip icequake activity in 2013 corresponds to a period of accelerating ice velocities (Figure 3a). While rift-tip fracture may be more directly related to strain rate in a viscous regime and strain in an elastic regime, we simply note that ice speed reflects the underlying stress state of the ice shelf. The correspondence in time between elevated rift-tip seismicity rates and increasing ice velocities therefore suggests that rift propagation is sensitive to the underlying stress state of the ice shelf. In addition, rift tip fracture may be enhanced by localized ice shelf thinning and melt within the rift. Christianson et al. (2016) hypothesize that the overall pattern of ice velocities at PIG in 2013 tracks a time-lagged response to ocean melting, and localized melt has been proposed as a primary driver of rifting at PIG (Walker & Gardner, 2019; Jeong et al., 2016). The observed connection in time between rift tip fracture and accelerated ice velocities demonstrates that rift growth and PIG is sensitive to changes in ice dynamics, localized melt, or a combination of both. At the present time, however, we are unable to confirm whether local or more distant melt-related feedbacks are responsible for the observed fracturing.

5.2 Rift/margin

The rift/margin icequakes are coincident in space and time with the growth of ~20 rifts formed in the northwest shear zone, as well as smaller-scale fractures and widening of the main rift itself. Rift/margin icequakes occurred more frequently in 2012 than in 2013. The mean seismicity rate was 27.7 icequakes/week in 2012 and 19.3 icequakes/week in 2013. Four weeks of 2012 equaled or exceeded the maximum 2013 seismicity rate of 70 icequakes/week. The timing of icequakes in the rift/margin group is independent of ice speed. Peak levels of rift/margin seismicity were observed during the week of May 15, 2012, which contained 109 rift/margin icequakes. Rift/margin icequakes reach peak seismicity rates in the weeks following the opening of the secondary rift branch in May 2012, suggesting that the crack opening caused aftershock-like seismicity and/or destabilized the margin, enhancing the growth of nearby fractures.

5.3 Shear margin

The shear-margin icequakes are coincident in space and time with the initiation of new cracks and growth of extant cracks near Evans Knoll. This area marks the transition from a primarily intact shear margin upstream of Evans Knoll to a highly fractured shear margin downstream of Evans Knoll. Imagery shows that multiple fractures longer than 1 km were initiated in this area during 2012 and 2013 (Figure 1). Shear-margin icequakes occurred at an approximately equal rate in 2012 and 2013. The mean seismicity rate was 31.9 icequakes/week in 2012 and 32.2 icequakes/week in 2013. Peak levels of shear margin seismicity were observed during the week of July 17, 2012, which contained 107 shear-margin icequakes. Shear-margin icequakes do not exhibit any prominent temporal trends and appear independent of ice velocity. The shear margin experiences the highest overall level of seismic activity, suggesting that the transition point from intact to fractured ice near Evans Knoll experiences higher stress concentrations than either the rift tip or the rift/margin regions, consistent with rift modeling (Lipovsky, 2020).

6 Icequake Source Analysis

We next estimate the distribution of forces that gives rise to the observed seismograms. We do this by removing wave propagation effects from the observed seismograms using a numerically computed Green's function. Our catalog was designed to represent icequakes that mostly consist of flexural gravity waves. We therefore model the vertical seismograms using the simplest model that gives rise to flexural gravity waves, the dynamic floating beam equation (Ewing & Crary, 1934; Squire & Allan, 1977),

$$\rho_i h_i \frac{\partial^2 w}{\partial t^2} + D \frac{\partial^4 w}{\partial x^4} + \rho_w g w + \rho_w \frac{\partial \phi}{\partial t} = P, \tag{1}$$
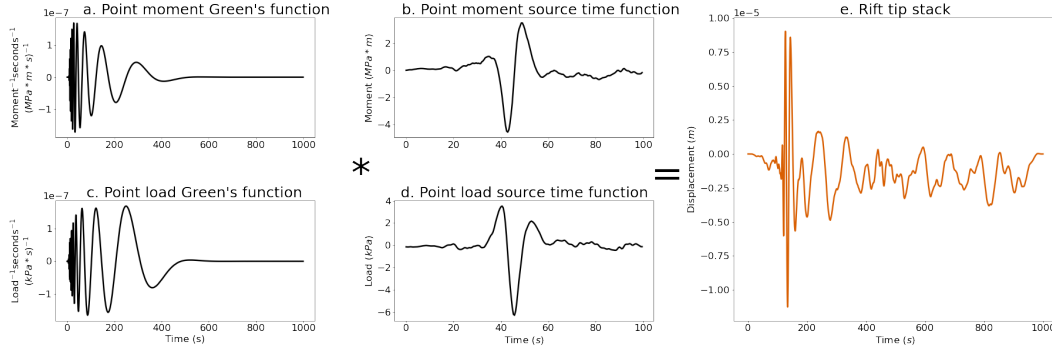
where $D \equiv EI = E h_i^3/[12(1-\nu^2)]$ is the flexural rigidity with second moment of area $I = \int_{-h_i/2}^{h_i/2} z^2 dz$, E is the Young's modulus of ice, ν is the Poisson's ratio of ice, t is time, x is horizontal position, g is gravitational acceleration constant, h_i is the ice thickness, ρ_i is the density of ice, ρ_w is the density of water, w is the vertical displacement of the beam, ϕ is the ocean surface velocity potential, and P is an applied point load. From left to right, the terms in Equation (1) represent inertia, flexure of the ice shelf, buoyancy, and ocean surface waves generated at the ice-water interface. We initially use a locally-averaged ice thickness of $h_i = 400$ m (Shean et al., 2019) and a water depth of $h_w = 590$ m (Fretwell et al., 2013).

We model icequake sources as either an applied point load or point bending moment. When a basal crevasse opens and fills with water, the downward-acting ice overburden stress at the top of the crevasse is greater in magnitude than the upward-acting buoyancy stress exerted by water filling the crevasse. This applies a downward point load to the ice shelf. In addition, the horizontal ice overburden stress along the walls of the crevasse is greater in magnitude than the horizontal buoyancy stress exerted by the water filling the crevasse. The difference in magnitude between these two stresses decreases with depth such that the walls of a crevasse are subject to stress gradient. This applies a bending moment to the ice shelf. These two mechanisms may act in concert and simultaneously apply a moment and point load to the ice shelf. We choose not to pursue such hybrid sources at the present time because the simplicity of our model –specifically the assumptions of uniform ice thickness and two-dimensional geometry– suggests that additional source complexity is not warranted prior to improvements in these other areas.

We obtain the Green's function of the floating beam equation as the impulse response of the mechanical system to a point load (force per unit length) source. Rewriting Equation 1 using the linear operator $\mathcal{A}$ as $\mathcal{A}w = P$, the Green's function equation can then be written as $\mathcal{A}G = \delta(x)\delta(t)$. In Supporting Text S4, we derive a frequency-wavenumber solution for G that we are able to analytically invert in the time domain and numerically invert in the frequency domain. We then derive G_m, the vertical displacement response to a point moment source.

We deconvolve G and G_m from waveform stacks to estimate the source load or moment distribution of events in each spatial group. Figure 4 shows our deconvolution result for the rift-tip icequakes, illustrating that a given vertical displacement seismogram may equivalently be represented as a point moment (Figure 4a and b) or a point load (Figure 4c and d). The equivalent analysis for the other two groups of events is given in Supporting Figures S1-2.

We examine the sensitivity of our deconvolution to the assumed value for the ice thickness by varying the ice thickness between 300 and 500 m (Figures S3-5). For the rift-tip group, we find source durations ranging from 30.48 to 50.00 s and amplitudes ranging from 2.69 to 6.90 MPa·m (point moment) and 3.83 to 8.62 kPa (point load). For the rift/margin group, we find source durations ranging from 19.52 to 48.57 s and amplitudes ranging from 3.82 to 12.55 MPa·m (point moment) and from 5.05 to 14.02 kPa (point

Figure 4. Green's functions and source time functions for rift tip events. (a) Theoretical Green's function for a point moment source located at a distance of 25 km, which is approximately the distance from PIG seismic array to the rift tip. (b) Source time function retrieved by deconvolving the point moment Green's function from the stack of rift tip vertical displacement waveforms. (c) Theoretical Green's function for a point load source located at a distance of 25 km. (d) Source time function retrieved by deconvolving the point load Green's function from the stack of rift tip vertical displacement waveforms. (e) Stack of rift tip vertical displacement waveforms obtained by aligning waveforms to a master event and taking the mean waveform on the frequency band 0.01-1 Hz.

266 load). Finally, for the shear-margin group, we find source durations ranging from 27.14
267 to 36.67 s and amplitudes ranging from 5.60 to 14.89 MPa·m (point moment) and from
268 8.04 to 12.97 kPa (point load).

7 Discussion of icequake source physics

270   How large were the cracks that generated the recorded flexural gravity waves? We
271 estimate the amount of vertical crack opening for each spatial group using the point load
272 source amplitudes (Text S5) for ice thickness varying between 300 and 500 m. Rift tip
273 point load amplitudes correspond to 4.3 to 9.8 m of vertical crevasse opening. Rift/margin
274 point load amplitudes correspond to 5.7 to 15.9 m of vertical crevasse opening. Shear-
275 margin point load amplitudes correspond to 9.1 to 14.7 m of vertical crevasse opening.
276 This suggests that the large-scale fracture opening and rift propagation observed in im-
277 agery (Figure 1) was the result of many discrete crack opening events that each spanned
278 only about 1 % of the ice thickness, not the result of full-thickness crack opening. Bassis
279 et al. (2007) and Heeszel et al. (2014) observed episodic rift seismicity on the Amery Ice
280 Shelf and proposed that rifts might propagate due to the coalescence of smaller cracks.
281 Our findings support the hypothesis that crack coalescence can act as a mechanism of
282 rifting.

283   Estimated source time series for moment and point load exhibit one or several pulses
284 of activity followed by a return to zero (Figure 4). Source time functions derived from
285 body waves in an elastic medium result in estimates of moment rate (Aki & Richards,
286 2002, Equation 4.32). Here, however, our deconvolution is sensitive not to the rate of change
287 of point load or moment, but instead to a point load and moment. This complicates the
288 interpretation of the estimated source time series because it suggests that the icequakes
289 represent the application and subsequent removal of some point load or moment. This
290 physically counterintuitive situation motivates an examination of the sensitivity of our
291 deconvolution to static offsets. We therefore calculate synthetic seismograms forced by
292 a step in moment or point load (Figures S6-S8). We find that in some cases the step func-

tion provides an acceptable fit to the observations. We therefore are unable to infer whether the observed flexural gravity waves were generated by a pulse-like or step-like source.

The timescale of the source process, however, is constrained independent of the exact force distribution assumed in the deconvolution. Our source analysis implies that the recorded flexural gravity waves were generated by fracturing process with approximately 20-50 s duration. At this timescale, the observed waves must have been generated by brittle fracture, not by viscous deformation. This 20-50 s timescale is extremely slow compared, for example, to tectonic earthquakes, where earthquake duration scales like $10^{M/2}$ with earthquake moment M and 20 s duration is associated with a $M = 7$ earthquake (Ekström et al., 2003).

What process sets the duration of the observed icequakes? The above scaling for tectonic earthquakes is based on the reasoning that the duration is set by the time required for a shear crack to propagate across a fault of length L at a rate that tends towards inertial velocities (either the shear or dilatational wave speed v_s or v_p) (Freund, 1998). In our system, however, we expect that water plays a limiting role in the speed of fracture propagation that may not be present in tectonic earthquakes. The propagation of fluid filled basal crevasses is expected to occur at the crack wave speed (Lipovsky & Dunham, 2015). The crack wave speed is much slower than the inertial velocities and could plausibly be in the range of 1-100 m/s for basal crevasses in ice shelves. These velocities would suggest source length scales on the order of meters to hundreds of meters. A second plausible explanation is that long durations may be explained by the coalescence of many smaller individual fractures that open successively. And yet another explanation is that there could be significant horizontal propagation which is not captured in our model. We expect that more detailed near-source observations would be able to distinguish between these possible scenarios.

8 Conclusions

We detect and locate icequakes that propagate as flexural gravity waves on the Pine Island Glacier ice shelf from 2012 to 2014. When compared to satellite imagery, the back-azimuthal distribution of the detected events suggests that the icequakes were generated by fractures at the tip of a large rift and in two distinct portions of the northern shear margin. Most of the events were generated at the shear margin near Evans Knoll, in agreement with imagery that suggests significant fracture initiation. Increased fracturing at the rift tip is associated with increased ice speed and elevated basal melting in 2013 (Christianson et al., 2016). We attribute this relationship to changes in the stress state of the ice shelf or to melt-driven thinning that elevated rift tip stress concentrations. We use a simple model of flexural gravity waves to constrain the source of the recorded waves. We find that the observed waves have a source duration between 20-50 s. This timescale implies that a brittle fracture process generated the waves. Our analysis therefore confirms the role of brittle processes in the long-term evolution of marine ice sheets.

References

Aki, K., & Richards, P. G. (2002). *Quantitative seismology.*

Allen, R. V. (1978, 10). Automatic earthquake recognition and timing from single traces. *Bulletin of the Seismological Society of America*, *68*(5), 1521-1532. Retrieved from `https://doi.org/10.1785/BSSA0680051521` doi: 10.1785/BSSA0680051521

Aster, R. C., Lipovsky, B. P., Cole, H. M., Bromirski, P. D., Gerstoft, P., Nyblade, A., ... Stephen, R. (2021). Swell-triggered seismicity at the near-front damage zone of the ross ice shelf. *Seismological Research Letters*.

Banwell, A. F., MacAyeal, D. R., & Sergienko, O. V. (2013). Breakup of the larsen b ice shelf triggered by chain reaction drainage of supraglacial lakes. *Geophysical Research Letters*, *40*(22), 5872–5876.

Bassis, J. N., Fricker, H. A., Coleman, R., Bock, Y., Behrens, J., Darnell, D., ... Minster, J.-B. (2007). Seismicity and deformation associated with ice-shelf rift propagation. *Journal of Glaciology*, *53*(183), 523–536. doi: 10.3189/002214307784409207

Bassis, J. N., Fricker, H. A., Coleman, R., & Minster, J.-B. (2008). An investigation into the forces that drive ice-shelf rift propagation on the amery ice shelf, east antarctica. *Journal of Glaciology*, *54*(184), 17–27. doi: 10.3189/002214308784409116

Benn, D. I., Warren, C. R., & Mottram, R. H. (2007). Calving processes and the dynamics of calving glaciers. *Earth-Science Reviews*, *82*(3-4), 143–179.

Bindschadler, R., Choi, H., Wichlacz, A., Bingham, R., Bohlander, J., Brunt, K., ... Young, N. (2011). Getting around antarctica: new high-resolution mappings of the grounded and freely-floating boundaries of the antarctic ice sheet created for the international polar year. *The Cryosphere*, *5*(3), 569–588. Retrieved from `https://tc.copernicus.org/articles/5/569/2011/` doi: 10.5194/tc-5-569-2011

Bromirski, P. D., Chen, Z., Stephen, R. A., Gerstoft, P., Arcas, D., Diez, A., ... Nyblade, A. (2017). Tsunami and infragravity waves impacting antarctic ice shelves. *Journal of Geophysical Research: Oceans*, *122*(7), 5786-5801. Retrieved from `https://agupubs.onlinelibrary.wiley.com/doi/abs/10.1002/2017JC012913` doi: https://doi.org/10.1002/2017JC012913

Chen, Z., Bromirski, P., Gerstoft, P., Stephen, R., Lee, W. S., Yun, S., ... Nyblade, A. (2019). Ross ice shelf icequakes associated with ocean gravity wave activity. *Geophysical Research Letters*, *46*(15), 8893–8902.

Christianson, K., Bushuk, M., Dutrieux, P., Parizek, B. R., Joughin, I. R., Alley, R. B., ... Holland, D. M. (2016). Sensitivity of pine island glacier to observed ocean forcing. *Geophysical Research Letters*, *43*(20), 10,817-10,825. Retrieved from `https://agupubs.onlinelibrary.wiley.com/doi/abs/`

396   10.1002/2016GL070500   doi: 10.1002/2016GL070500

397 Clerc, F., Minchew, B. M., & Behn, M. D.   (2019).   Marine ice cliff instability mit-
398   igated by slow removal of ice shelves.   *Geophysical Research Letters*, *46*(21),
399   12108–12116.

400 David Holland, & Robert Bindschadler.   (2012).   *Observing pine island glacier (pig)*
401   *ice shelf deformation and fracture using a gps and seismic network.*   Interna-
402   tional Federation of Digital Seismograph Networks.   Retrieved from `https://`
403   `www.fdsn.org/networks/detail/XC_2012/`   doi: 10.7914/SN/XC_2012

404 Ekström, G., Nettles, M., & Abers, G. A.   (2003).   Glacial earthquakes.   *Science*,
405   *302*(5645), 622–624.

406 Ewing, M., & Crary, A. (1934). Propagation of elastic waves in ice. part ii. *Physics*,
407   *5*(7), 181–184.

408 Fretwell, P., Pritchard, H. D., Vaughan, D. G., Bamber, J. L., Barrand, N. E.,
409   Bell, R., ... Zirizzotti, A.   (2013).   Bedmap2: improved ice bed, surface
410   and thickness datasets for antarctica.   *The Cryosphere*, *7*(1), 375–393.   Re-
411   trieved from `https://tc.copernicus.org/articles/7/375/2013/`   doi:
412   10.5194/tc-7-375-2013

413 Freund, L. B. (1998). *Dynamic fracture mechanics*. Cambridge university press.

414 Gibbons, S. J., & Ringdal, F.   (2006, 04).   The detection of low magnitude seis-
415   mic events using array-based waveform correlation.   *Geophysical Journal Inter-*
416   *national*, *165*(1), 149-166.   Retrieved from `https://doi.org/10.1111/j.1365`
417   `-246X.2006.02865.x`   doi: 10.1111/j.1365-246X.2006.02865.x

418 Hammer, C., Ohrnberger, M., & Schlindwein, V. (2015). Pattern of cryospheric seis-
419   mic events observed at ekström ice shelf, antarctica. *Geophysical Research Let-*
420   *ters*, *42*(10), 3936–3943.

421 Heeszel, D. S., Fricker, H. A., Bassis, J. N., O'Neel, S., & Walter, F.   (2014).   Seis-
422   micity within a propagating ice shelf rift: The relationship between icequake
423   locations and ice shelf structure.   *Journal of Geophysical Research: Earth*
424   *Surface*, *119*(4), 731-744.   Retrieved from `https://agupubs.onlinelibrary`
425   `.wiley.com/doi/abs/10.1002/2013JF002849`   doi: 10.1002/2013JF002849

426 Hulbe, C. L., LeDoux, C., & Cruikshank, K.   (2010).   Propagation of long frac-
427   tures in the ronne ice shelf, antarctica, investigated using a numerical model
428   of fracture propagation.   *Journal of Glaciology*, *56*(197), 459–472.   doi:
429   10.3189/002214310792447743

430 Jeong, S., Howat, I. M., & Bassis, J. N.   (2016).   Accelerated ice shelf rift-
431   ing and retreat at pine island glacier, west antarctica.   *Geophysical Re-*
432   *search Letters*, *43*(22), 11,720-11,725.   Retrieved from `https://agupubs`
433   `.onlinelibrary.wiley.com/doi/abs/10.1002/2016GL071360`   doi:
434   https://doi.org/10.1002/2016GL071360

435 Joughin, I., Shapero, D., Dutrieux, P., & Smith, B. (2021). Ocean-induced melt vol-
436   ume directly paces ice loss from pine island glacier.   *Science advances*, *7*(43),
437   eabi5738.

438 Joughin, I., Shapero, D., Smith, B., Dutrieux, P., & Barham, M.   (2021).   Ice-shelf
439   retreat drives recent pine island glacier speedup.   *Science Advances*, *7*(24),
440   eabg3080.

441 Larour, E., Rignot, E., & Aubry, D.   (2004).   Modelling of rift propagation on ronne
442   ice shelf, antarctica, and sensitivity to climate change. *Geophysical research let-*
443   *ters*, *31*(16).

444 Lipovsky, B. P. (2018). Ice shelf rift propagation and the mechanics of wave-induced
445   fracture.   *Journal of Geophysical Research: Oceans*, *123*(6), 4014-4033.   doi:
446   https://doi.org/10.1029/2017JC013664

447 Lipovsky, B. P. (2020). Ice shelf rift propagation: stability, three-dimensional effects,
448   and the role of marginal weakening.   *The Cryosphere*, *14*(5), 1673–1683.   doi:
449   10.5194/tc-14-1673-2020

450 Lipovsky, B. P., & Dunham, E. M. (2015). Vibrational modes of hydraulic fractures:

Inference of fracture geometry from resonant frequencies and attenuation. *Journal of Geophysical Research: Solid Earth*, *120*(2), 1080–1107.

MacAyeal, D. R., Okal, E. A., Aster, R. C., & Bassis, J. N. (2009). Seismic observations of glaciogenic ocean waves (micro-tsunamis) on icebergs and ice shelves. *Journal of Glaciology*, *55*(190), 193–206.

MacGregor, J. A., Catania, G. A., Markowski, M. S., & Andrews, A. G. (2012). Widespread rifting and retreat of ice-shelf margins in the eastern amundsen sea embayment between 1972 and 2011. *Journal of Glaciology*, *58*(209), 458–466.

Mattsson, K., Dunham, E. M., & Werpers, J. (2018). Simulation of acoustic and flexural-gravity waves in ice-covered oceans. *Journal of Computational Physics*, *373*, 230–252.

McGrath, D., Steffen, K., Scambos, T., Rajaram, H., Casassa, G., & Lagos, J. L. R. (2012). Basal crevasses and associated surface crevassing on the larsen c ice shelf, antarctica, and their role in ice-shelf instability. *Annals of glaciology*, *53*(60), 10–18.

Olinger, S. D., Lipovsky, B. P., Wiens, D. A., Aster, R. C., Bromirski, P. D., Chen, Z., . . . Stephen, R. A. (2019). Tidal and thermal stresses drive seismicity along a major ross ice shelf rift. *Geophysical Research Letters*, *46*(12), 6644-6652. Retrieved from https://agupubs.onlinelibrary.wiley.com/doi/abs/10.1029/2019GL082842 doi: 10.1029/2019GL082842

Paparrizos, J., & Gravano, L. (2016, June). K-shape: Efficient and accurate clustering of time series. *SIGMOD Rec.*, *45*(1), 69–76. Retrieved from https://doi.org/10.1145/2949741.2949758 doi: 10.1145/2949741.2949758

Pitz, W., & Miller, D. (2010). The terrasar-x satellite. *IEEE Transactions on Geoscience and Remote Sensing*, *48*(2), 615-622. doi: 10.1109/TGRS.2009.2037432

Renshaw, C. E., & Schulson, E. M. (2001). Universal behaviour in compressive failure of brittle materials. *Nature*, *412*(6850), 897–900.

Rist, M., Sammonds, P., Oerter, H., & Doake, C. (2002). Fracture of antarctic shelf ice. *Journal of Geophysical Research: Solid Earth*, *107*(B1), ECV–2.

Scambos, T. A., Bell, R. E., Alley, R. B., Anandakrishnan, S., Bromwich, D., Brunt, K., . . . others (2017). How much, how fast?: A science review and outlook for research on the instability of antarctica's thwaites glacier in the 21st century. *Global and Planetary Change*, *153*, 16–34.

Sergienko, O. (2017, 07). Behavior of flexural gravity waves on ice shelves: Application to the ross ice shelf. *Journal of Geophysical Research: Oceans*, *122*. doi: 10.1002/2017JC012947

Seroussi, H., Nowicki, S., Payne, A. J., Goelzer, H., Lipscomb, W. H., Abe-Ouchi, A., . . . others (2020). Ismip6 antarctica: a multi-model ensemble of the antarctic ice sheet evolution over the 21st century. *The Cryosphere*, *14*(9), 3033–3070.

Shean, D. E., Joughin, I. R., Dutrieux, P., Smith, B. E., & Berthier, E. (2019). Ice shelf basal melt rates from a high-resolution digital elevation model (dem) record for pine island glacier, antarctica. *The Cryosphere*, *13*(10), 2633–2656. Retrieved from https://tc.copernicus.org/articles/13/2633/2019/ doi: 10.5194/tc-13-2633-2019

Shepherd, A., Ivins, E., Rignot, E., Smith, B., Van Den Broeke, M., Velicogna, I., . . . others (2018). Mass balance of the antarctic ice sheet from 1992 to 2017. *Nature*, *558*, 219–222.

Squire, V. A., & Allan, A. (1977). *Propagation of flexural gravity waves in sea ice.* Centre for Cold Ocean Resources Engineering, Memorial University of Newfoundland.

Stanton, T. P., Shaw, W., Truffer, M., Corr, H., Peters, L., Riverman, K., . . . Anandakrishnan, S. (2013). Channelized ice melting in the ocean boundary layer beneath pine island glacier, antarctica. *Science*, *341*(6151), 1236–1239.

Von der Osten-Woldenburg, H. (1990). Icequakes on ekström ice shelf near atka bay, antarctica. *Journal of Glaciology*, *36*(122), 31–36.

Walker, C., & Gardner, A. (2019). Evolution of ice shelf rifts: Implications for formation mechanics and morphological controls. *Earth and Planetary Science Letters*, *526*, 115764. Retrieved from https://www.sciencedirect.com/science/article/pii/S0012821X1930456X doi: https://doi.org/10.1016/j.epsl.2019.115764

Weertman, J. (1973). Can a water-filled crevasse reach the bottom surface of a glacier. *IASH publ*, *95*, 139–145.

Williams, R., & Robinson, E. (1981). Flexural waves in the ross ice shelf. *Journal of Geophysical Research: Oceans*, *86*(C7), 6643–6648.

Winberry, J. P., Huerta, A. D., Anandakrishnan, S., Aster, R. C., Nyblade, A. A., & Wiens, D. A. (2020). Glacial earthquakes and precursory seismicity associated with thwaites glacier calving. *Geophysical Research Letters*, *47*(3), e2019GL086178. Retrieved from https://agupubs.onlinelibrary.wiley.com/doi/abs/10.1029/2019GL086178 (e2019GL086178 2019GL086178) doi: 10.1029/2019GL086178

Zhan, Z., Tsai, V. C., Jackson, J. M., & Helmberger, D. (2014). Ambient noise correlation on the amery ice shelf, east antarctica. *Geophysical Journal International*, *196*(3), 1796–1802.